Structural Investigation, Chemical Durability, And Kinetic Characterization of Sodium-Tungsten-Titanium Phosphate Glasses

Hicham Es-soufi (hichamessoufi@gmail.com)
Faculté des Sciences de Meknès, Université Moulay Ismail https://orcid.org/0000-0002-2075-1376
L. Bih
Faculté des Sciences de Meknès, Université Moulay Ismail

Research Article

Keywords: phosphate glasses, crystallization kinetics, durability, solid electrolytes

Posted Date: January 18th, 2022

DOI: https://doi.org/10.21203/rs.3.rs-1033051/v1

Abstract

Solid electrolytes of sodium ions were applied in many technologies, from chemical sensors to batteries. In this work, we focused on the study of electrolytes-based phosphate glasses prepared within the system $20Na_2O$-$(50-x)Na_2WO_4$-$xTiO_2$-$30P_2O_5$ (with $0 \leq x \leq 25$ mol%). These glasses were elaborated via a melt-quenching method. The DSC technique was exploited to estimate the activation energy depending on the crystallization (E_c). Where the glass (x= 5) was characterized by E_c= 144.77 kJ/mol. Avrami parameter (n) allows determining the mechanism of crystallization. This parameter value is found around $\approx$ 2; it can anticipate that the crystallization mechanism is a one-dimensional, periodic landscape. The Raman spectroscopy analysis showed that the bonds constituting the framework of these glasses are essential constituted from the PO_4 units. The insertion of TiO_2 into the glass framework leads to formation of the new bonds P-O-Ti and/or Ti-O-Ti. Changing the Na_2WO_4 mol% by TiO_2 mol% leads to switching the structural units Q^2 to Q^1 units then Q^0 units. Obtained results of the durability analysis verified that the dissolution of the explored glasses relies on glassy composition. When TiO_2 replaces Na_2WO_4, durability is increased.

1. Introduction

Many researchers are interested in sodium-ion batteries, because of their low cost and high energy density, in comparing them with their similar, lithium-ion batteries [1–4]. The processes of the ionic conductivity into the electrolyte have been developed at room temperature, in addition to the development of electrochemical stability windows [5]. For this reason, sodium-ion systems have great potential as the future large-scale power sources for different applications. Many published works have been consolidated on the status of liquid, polymer gel, and solid electrolytes. In addition, all parameters (electrochemical stability, ionic conductivity, viscosity, thermal characteristics) influencing the applications of these electrolytes of the sodium-ions were discussed in many previous works [6–8].

As well known, an electrolyte is a medium responsible for ionic transport, typically for Na^+ ion transport in electrolytes of the sodium ions, and hence controls the power density. Ionic conductivity is an interesting property for the electrolyte. The electronic conductivity of the electrolytes must be negligible to evade short-circuit. Besides, electrolytes should have good stability (mechanical, electrochemical, thermal, etc.), alongside excellent interfacial properties. However, the lowest and highest molecular orbital energy levels in the electrolyte were determined in the thermal and voltage stability ranges of the battery [10]. The main question of present-day research efforts counts on evolving suitable electrolytes applied at ambient temperature. To fabricate room-temperature-rechargeable SIBs, electrolytes with relatively high Na^+ ion conductivity and the capacity to format more appropriate electrode-electrolyte interfaces are indispensable. Recently, Sawiki et al have reported progress in electrode materials and solid electrolytes adequate for sodium ion batteries [11]. Recently, many publications have clearly revealed that there is significant and unprecedented growth in research around the world on electrolytes for SIBs. Conceptually, the possibility of these SIBs has been proved several years ago [12].Recently, the topic of looking at

alternatives for lithium systems, it become an urgent need. In spite of some initiatives interested in sodium-ion batteries like; Na-S and Na-$NiCl_2$ employed the $NaAl_{11}O_{17}$ as a ceramic electrolyte [13–16].

Amorphous materials based on sodium phosphate are good candidates as solid electrolytes in sodium batteries [17–20]. As well known, sodium phosphate glasses are generally characterized by poor chemical stability. For this reason, the chemical durability parameter is a crucial determinant in solid electrolytes. According to the literature, the reaction between the glass and water is produced in two steps: i) diffusion process; the ionic exchange between Na^+ close to non-bridging oxygens (NBO) and the protonated species, which is proportional to $t^{1/2}$. ii) during the hydrolysis process; it occurs the rupture of the P–O–P chain phosphates depends upon the time (t) [21–23]. The solubility of phosphate glasses containing metal oxides has been improved by researchers to investigate their effects on the chemical, physical, and mechanical properties [27–29]. Besides, all studies have been reported that incorporation of the metals has enhanced the durability of the phosphate glasses [30–31]. Especially, these glasses meet a global problem that depends on poor solubility. In this context, metal oxides explored their influence on the structure and physic-chemical properties of phosphate glasses. It confirmed that the insertion of metals led to improving the durability of the studied glasses. Recently, titanium has taken a lot of consideration; as a result of its good stabilizer, the phosphate framework, by forming the new Ti–O–P bonds in the place of the P–O–P bonds [32–34]. Many works have reported that titanium dioxide effectively enhances the degradability of glassy phosphates [35–38]. As well known, titanium oxide acts as an intermediary (modifier, or former), but cannot form a glass alone [33]. The titanium ion can easily modify the structure and the characteristics of the host glass, because the titanium ion is differentiated by a small ionic size [39]. Also, titanium exists in the form of the two valence states; trivalent Ti^{3+} of the purple color and tetravalent Ti^{4+} colorless [39]. In most cases, titanium Ti exists as a six-coordinated form in the structural phosphate, besides five and four-coordinated forms [33]. The glassy phosphates of the titanium are intensively reported in many publications for their possibility to apply them in interesting technologies. Because of their titanium–phosphate glasses have great electrical, optical, and magnetic properties [39]. Besides, phosphate glasses of the tungsten are great materials, because they present good photochromic, gasochromic, and electrochromic properties [40]. Generally, high WO_3 mol% (60–75 mol %) can form glasses in binary systems with glass-forming, such as GeO_2, B_2O_3, and P_2O_5. Where WO_3 content (up to 80 mol%) allowed to form a stable binary P_2O_5–WO_3 [40]. Characterization of glasses containing WO_3 shows that the existence of the tungsten ions in octahedral coordination has been confirmed [41]. Besides, structural studies showed that the WO_6 octahedra and PO_4 tetrahedral share their corners in tungstophosphate glasses, a binary system. However, the glasses represented by 80 mol% of WO_3 are not stable, because these glasses are dominant by octahedrals shared in the corner. Where, these glasses are susceptible to crystallization [41]. But the glassy system $SbPO_4$–WO_3 presents good stability in addition to their highest refraction index [42]. The structural data checked that the WO_6 octahedra can determine two glass frameworks. The first one is focused on the bridging of the PO_4 tetrahedra with the WO_6 octahedral forward of the structure. The second one is created jointly by the both WO_6 octahedral, when WO_3 increased [42]. The glassy phosphates are vitrified in a broad range of

compositions within the P_2O_5–WO_3–A_2O ternary diagrams (A = Na, Li). The structural investigation of modified glassy phosphates of the P_2O_5–A_2MO_4–A_2O ternary system (M = Mo, W; A = Li, Na) is investigated through using Raman, infrared, and RPE spectroscopies. These glasses contain in their structure MO_6 octahedral, MO_4 tetrahedral, M_2O_7 dimmers, PO_4 and P_2O_7 units or metaphosphate chains established on the glassy composition considered. It is shown that the vitreous framework is depolymerized when the quantity of A_2O increases. RPE experiments were released on samples irradiated and not irradiated by X-ray diffraction [43]. Glasses belonging to the series $yA_2O–(1–y)$ $[0.25(WO_3)_2–0.75P_2O_5]$ (y = 0.10–0.60) are produced. ATD experiments expose that the glassy network is broken with increasing modifier content. The RPE spectra show the existence of two signals dependent on the W^{5+} and Mo^{5+} ions. The intensity of these RPE centers decreases when the amount of A_2O increases. Decreasing in T_g with the amount of the oxide modifier is associated with structural changes occurring in the matrix of these glassy compositions [44]. This work aims to study the structure and chemical durability of solid electrolytes constituted from the phosphate glasses ($20Na_2O–(50–x)Na_2WO_4–TiO_2–30P_2P_5$; x= 0–25 mol %) containing different quantities of TiO_2 mol%. The effect on chemical stability through the insertion of a TiO_2 mol% from 5 mol% to 25 mol% has been analyzed and depended on the variation of the structure of phosphate glasses over the demineralized water at 30°C.

2. Materials And Methods

2. 1 Glass Preparation

Phosphate glasses with the formula of $20Na_2O–(50–x)Na_2WO_4–xTiO_2–30P_2O_5$ (x=0, 1, 5, 8, 10, 15, 20, and 25 mol%) were prepared by conventional melt-quenching route, from the precursors Na_2CO_3, Na_2WO_4, TiO_2, $NH_4H_2PO_4$ (purchased from Sigma-Aldrich, USA) were weighed and mixed thoroughly according to appropriate molar compositions. The mixture was placed in an alumina crucible in a furnace, and then it was first heated at 300°C per 12 hours and 500°C per hour. After that the value of the temperature, the electrical furnace was increased to attain the melt and was stirred for homogenization for about 1 hour at 900°C, the preparation temperature. After quenching the melt in the air to obtain the glasses which are annealed after that at 300°C for one hour, then cooled down until room temperature, in the electric furnace. By process, the prepared glasses were obtained transparent and colorless, so they were put in desiccators before use. The amorphous state of the obtained glasses was analyzed by X–ray Diffractometer and confirmed by using Raman spectroscopy.

2. 2. Glass Characterization

The Raman technique was investigated to check the structural framework of the phosphate units of the prepared glasses. The Raman data were collected at ambient temperature using a Horiba Jobin Yvon Lab Ram HR spectrometer. The spectra were analyzed in backscattering geometry under excitation with He–

Ne laser radiation (632.8nm) at a power of 12 mW. The exposure time was 3 s, the accumulated number was 10, and the spectral slit width was 1mm.

Chemical durability data for the elaborated glasses were determined from dissolution tests, which were carried out in demineralized water at 30°C. The obtained glasses are formed in blocks form, then putted into a bottle already full of demineralized water characterized by pH= 6.8. The bottles are fixed in a thermostatic bath. Where, the thermostat is regulated at 30˚C for 250 hours. The percentage of the dissolution (DR) is determined by the equation DR= Dx/(S.t). Where; Dx, S, and t are, respectively, the mass loss (g), surface (cm^2) of the sample and initial state, and time of immersion (min). Through determination of the rate of the dissolution at each 24 hours, it also measured the pH of the leaching solution of the each glass by a pH-meter.

Data on the kinetics of the crystallization were collected by the DSC technique, at temperatures between 30°C and 550°C. The synthesized glasses are grounded to obtain the fine powder (< 50µm), then weighted 40mg of the fine powder to place it in a small aluminum crucible, and then heated at a 5°C/min, 8°C/min, 10°C/min, and 12°C/min. The collected data were used to fix the value of the peak crystallization temperature (T_p) at each rate β (°C/mn^{-1}).

3. Results And Discussion

3. 1. Raman spectroscopy

The structure of prepared glassy phosphates of the system $20Na_2O–(50–x)Na_2WO_4–xTiO_2–30P_2O_5$ (x= 0, 1, 5, 8, 10, 15, 20, and 25 mol%) were studied by using Raman scattering, spectroscopy, which carried out in the wavenumber range between 1200 cm^{-1} and 150 cm^{-1} and the results are gathered in Figure 1. The bands of the Raman spectra are attributed according to literature [45–47]. Therefore, the principal band positions and their attributions are gathered in Table 1. Where the main bands are checked at different positions: 1095 cm^{-1}, 935 cm^{-1}, 885 cm^{-1}, 750 cm^{-1}, 650–570 cm^{-1}, 390 cm^{-1} and 255 cm^{-1}. From Figure 1, it was observed that the main bands were located from 935 cm^{-1} to 750 cm^{-1}. These are associated with asymmetric and symmetric vibration modes of non-bridging oxygen on different P–tetrahedra. Besides, the systematic decrease in peak frequency for P–O bonds on 3–dimensional phosphates (Q^2), P_2O_7 (Q^1) dimer and isolated PO_4 (Q^0). The band around 885 cm^{-1} is associated with the symmetric vibration mode of the W–O bond of the WO_6 and/or W–O–P bond. The band of low intensity, located at 750 cm^{-1}, is associated with the symmetric vibration modes of the P–O–P bond of the Q^1 units also appeared. The bands located in the low region between 650 cm^{-1} and 255 cm^{-1}, are generally assigned as stretching modes of the [PO_4] units.

Table 1

Raman band assignments in the 1200–150 cm^{-1} range frequency for the studied phosphate glasses.

Band position (cm^{-1})	Band assignment
1095	$v_s(PO_2)^-$, Q^2
935	v_{as}(P–O–P)/ v_{as}(P–O–M) (M= W. Ti)
885	O–M–O/MO_4/MO_6 (M= W. Ti)
750	v_s(P–O–P), Q^1
650–570	v_s(P–O–P), Q^2
390	v_s(M–O–M)(M= W, Ti)
255	δ δ(PO_4)

Even after the substitution of Na_2WO_4 by TiO_2 in the system, it appeared that the spectra have changed significantly with an increasing of TiO_2 content. From composition (x= 1 mol%), it was observed that two supplementary bands at 935 cm^{-1} and 885 $cm^{-1}$are, respectively, dependent on the TiO_4 and TiO_6. That their intensities decreased at TiO_2 mol% increased (region marked with red color, Figure 1) [48]. The relative intensity of the peak assigned to Q^1 decreased when TiO_2 content increased. Besides, it looked that the intensity of the bands between 450 cm^{-1} and 180 cm^{-1} started decreasing when the quantity of TiO_2 increased (region marked with green color as mentioned in Figure 1).

At increasing TiO_2 content increased up to 5 mol% and more, the band in the position 1095 cm^{-1} was observed with an intensity decreasing with increasing the quantity of TiO_2. The vibrations in a range from 1050 cm^{-1} to 1095 cm^{-1} are associated with the symmetric vibration mode of nonbridging oxygens in pyrophosphate structural units $(P_2O_7)_4^-$ [49]. In the region of lower wave numbers, a band at 650 cm^{-1} is observed; the intensity decreases with increasing content of TiO_2. According to literature [50], it could be designed to control the vibration mode of Ti–O bonds in TiO_6 octahedral units. It can be predicted by the existence of several structural units in different glassy frameworks. Besides, some suggestions showed that the titanium ions could be occupied by distorted octahedrals, which contributed to the modification glassy matrix, and then the NBOs increased. Because of the existence of TiO_2 mol% in high quantities (x> 5), the structural units TiO_4 break the P=O bonds, which leads to the forming of new non–bridging oxygen ions. The structural units $[TiO_{6/2}]^2$ will be formed [51]. In additions, the TiO_6 structural units increase at high TiO_2 quantities.

From the analysis Figure 1, the Raman spectra attributed, the vibration intensity identifying the metaphosphate Q^2 units is significantly reduced up to x = 8 mol% and the pyrophosphate Q^1 units predominate for $x \geq 8$. But the exact determination, the quantity of Q^1 and Q^2 units is difficult. Also, the higher polarizability of the Ti–O bonds compared with the P–O bonds has been influenced by the intensity attributed to Raman bands. In spite of increasing TiO_2 to 20 mol% and 25 mol%, it can find glassy phosphates that have the metaphosphate Q^2 units [50]. It assumes that increasing the TiO_2 mol% in the glassy framework led to partly changing the metaphosphate structure to a pyrophosphate, then an orthophosphate. At a quantity of TiO_2 (x<8 mol%) the metaphosphate units are predominant in the glassy structural. After that, the pyrophosphate units will be raised, also the orthophosphate units. Therefore, the TiO_6 units interlink with different phosphate units (metaphosphate, pyrophosphate and orthophosphate) leading to formation of new bonds P–O–Ti, which participate to increase the durability for prepared glasses (see section 3.2).

3. 2. Chemical durability

3. 2. a. Weight loss

Glassy phosphates of simple compositions are very vulnerable. Their corrosion resistance changes only very slightly with condensation. Certainly an improvement appears in the polyphosphate → metaphosphate → ultraphosphate series associated with the finding of the phosphorus atoms at the Q^3 site, slowing the water diffusion step-by-steric effect. However, the durability of these compositions remains insufficient to hope for potential applications. An effective improvement involves an increase in the cross-linking of the phosphate entities, which form the glassy network to make it as tight as possible to aqueous attacks. To develop phosphate glasses resistant to corrosion by water, it is necessary to choose not only the type of phosphate anions which will be used for the structural building, but also the addition cations or the substitution anions. A compromise between these glassy components makes it possible to optimize the cross-linking of the entity phosphates while taking care to obtain vitrifiable compositions [52–53].

Data collected from durability tests are given in curve forms, as seen in Figure 2. Where, the weight loss at the initial surface ($g.cm^{-2}$) is dependent on the time (h). For the first time, it was observed that the glasses had the same dissolution behavior (see Figure 2). To simplify knowing the curve variation, it followed, one method is based on dividing the curves. For this reason, it could separate into two regions: the first one is at t<100h, where the dissolution is dominated by a linear behavior. But, the second one, between 100h and 250h, which is scarred by a slow-down in the dissolution rate. Regarding the substitution of Na_2WO_4 by TiO_2, it was checked the dissolution comportment of the synthesized glasses banks on the TiO_2 mol%. At the initial situation of dissolution of the glassy composition (x = 0 mol%), the dissolution was faster than other glassy compositions (x> 0 mol%). Because of this, it could conclude that the substitution of Na_2WO_4 by TiO_2 influences the solubility of the studied glasses. Furthermore, insertion of TiO_2 mol% in glassy phosphate improved the durability of glassy framework. In previous studies, it has been tested

some oxides; Fe_2O_3 and TiO_2 for improving the durability of the glassy phosphates [54–55]. From these previous works, it has been concluded that the insertion of Fe_2O_3 or TiO_2 into glassy networks enhanced the durability by the creation of a new P–O–Fe/Ti bonds, which lead to increasing of network rigidity. For similar roads, the insertion of different quantities of the quantity of the TiO_2 into our studied glasses has improved of durability of the studied glassy network, through creation of new P–O–Ti bonds. This hypothesis was corroborated by Raman spectroscopy, by identification of the new bonds (P–O–Ti). Also, it was confirmed by thermal examination (DSC). Where, at the integration of TiO_2 in glassy networks, T_g increased.

Insertion of TiO_2 into glasses improves the strengthening of the chains formed in the glassy network of the $Na_2O–Na_2WO_4–TiO_2–P_2O_5$ system. This explanation is supported through the correlation of chemical durability with thermal and Raman analysis.

3. 2. B. Ph Variation

Corrosion by water of alkaline phosphate glasses of compositions $(1–x)P_2O_5–xNa_2O$) can be summed up by the involvement of two mechanisms (hydration and hydrolysis) The importance of each one varies as a function of composition (x) and the degree of depolymerization [52]. Hydration is connected to the diffusion of water, forming a hydration layer. Hydration is predominant when the glassy structure consists mainly of Q^2 units forming chains, i.e. around x = 0.5 (metaphosphate and polyphosphate). It generally begins with the chain ends formed by hydroxylated Q^1 entities, giving free access to penetration of water between the chains. Well-known that the hydrated chains detach intact from the glassy surface to migrate into the solution. But the hydrolysis mechanism is characterized by:

i) low-energy reaction when it is an interdiffusional phase with an ion-exchange reaction $H^+ \leftrightarrow Na^+$, called "dealkalinization" or "ion-exchange", between the ions of the solution and the Na^+ ions located among the phosphate entities;

ii) much more energetic reaction regarding causing the rupture of a P–O–P bond with binding of H^+ and OH^- ions from the dissociation of water. It is in particular responsible for dissolving the ultraphosphates. But the chains were relieved into the solution, starting with their ends [52].

Figure 3 exposes the evolution of the pH curves as a function of the submersion time in demineralized water at a temperature of 30 ° C. In the same way, for analyzing the curves of chemical durability, it's going to analyze the pH curves. From the pH curves, it could be clearly differentiated into two regions: i) at t<48 h it's characterized by a hard decrease in pH curves; ii) at 48 h>, the pH curves show a horizontal linear (behavior is nearly constant) with a distinction among the curves of the studied glasses. From this attitude of the curves, it can be suggested that the development of pH values is established on the chemical composition of the glassy studied. In the literature, the evolution of pH is affected by the forming of phosphoric acid, which is survived by the $H_2PO_4^-$ units, in water [54]. Generally, through first

contact, the glass with the solution (water), the alkali ions and the phosphate ions created on the glassy surface have been leached into the solution. Therefore, the ion interchange between ions formed on the glassy surface and those of a solution; it could determine the acid–base character of the solution. In effect, the sudden decrease in pH curves associated with the influx of the phosphate units ($H_2PO_4^-$) from glassy surface to the solution (first region). But when the $H_2PO_4^-$ units slowdown because of saturation of the solution, the pH curves behavior becomes constant (second region). At TiO_2 mol% increased (x>5) into the glassy network. The pH curves decreased (only for the first region). But for the second region, saturation rapidly happened, as the quantity of TiO_2 increased. Because of this, it was verified that the insertion of the TiO_2 mol% into the glassy framework enhanced the durability for the studied glasses.

In conclusion, our study of chemical durability interested in the produced glasses could distinguish between two regions: the first one is described by a rapid alteration. Where thermodynamic disequilibrium happens between the glassy surface and the changing solution is important, which leads to an abrupt decrease in the pH value. The second one, is dominated by corrosion, which is checked with the saturation of the altering solution. Where, the saturation phenomenon has happened because of the founding of the protective layer against diffusion on the glassy surface.

2. 3. Crystallization Kinetics By Dsc

Thermal analysis of glasses by DSC makes it prospective to identify their behavior as a function of temperature. When we analyze glasses using several heating speeds (β), we can get information on their crystallization. From these non-isothermal measurements, we can follow the development of the crystallization temperature as a function of the heating rate (Tc= (β)).This variation allowed us to decide the parameters characterizing the crystallization of materials, including the activation energy of the crystallization (Ec).

The activation energy of the crystallization (E_c) is determined from the decide form of Kissinger equation (1), which was reported by Matusita and Saka [56]. This crystallization activation energy (Ec) will be investigated to establish the crystallization kinetics mechanism of the studied glasses.

$$Ln(T^2_p/\beta) = E_c/(RT_P) + \text{constant} \quad (1)$$

Where; β, R and T_p are, respectively, the heating rate β (5°C/min, 8°C/min, 10°C/min, 12°C/min), the universal gas constant, and the peak temperature.

From the value of the activation energy (E_c), the Avrami exponent (n) was calculated using Augis–Bennett equation (2) [57]:

$$n = (2.5/\Delta T)\times(RT^2_P/E_c) \quad (2)$$

With; n and ΔT are, respectively, the crystallization index or Avrami exponent and the full width of the exothermic DSC peak at half-maximum intensity. The Avrami exponent (n) indicated the growing and nucleation mechanisms. In the literature, (n) is nominated to crystallization pattern, n= 1 designed to surface crystallization, n= 2 means mono-dimensional crystallization, n= 3 means bi-dimensional crystallization, n= 4 designs to crystallization for glassy materials were in three-dimensional [58–59].

Figure 4 exhibits the DSC thermograms corresponding to the glassy formulation (x= 5) for all suggested heating rates. It was checked that each DSC thermogram presented a crystallization peak. But in comparison between the crystallization peaks, it noted, slowly shifted to the superior temperature value as heating rates increased. The obtained values, corresponding crystallization temperature (T_p) of the synthesized glass (x = 5 mol %) are gathered in Table 2. By examination of the crystallization temperature (T_p) and heating rates, it has been achieved from the Figure 5, which exposes the plot of $\ln(Tp^2/\beta)$ versus $1/T_p$. Also, it could be determined E_c from the slope of the variation, the parameter $\ln(Tp^2/\beta)$ as a function of $1/T_p$. The obtained E_c value is around ≈ 144.77 kJ/mol. The Avrami parameter (n) is found to be about 2, which suggests that the crystallization of the prepared glasses is controlled by a mono-dimensional mechanism [60–62].

Table 2
Crystallization temperature of the glass (x = 5 mol %) at different heat crystallization rates.

Glass	β(°C/min)	T_p	ΔT	Avrami parameter (n)
$20Na_2O–45Na_2WO_4–5TiO_2–30P_2O_5$	5	558	18	2.43
	8	566	20	2.25
	10	570	21	2.17
	12	573	23	2.01

Conclusion

Author contributions

H. Es-soufi: Conceptualization, Writing - review & editing. **L. Bih**: Validation

Conflict of Interest

The authors declare that they have no conflict of interest

Declarations

Author contributions

H. Es-soufi: Conceptualization, Writing - review & editing. **L. Bih**: Validation

Conflict of Interest

The authors declare that they have no conflict of interest

References

1. Fergus, J.W.: (2012). 227, 102-112. https://doi.org/10.1016/j.ssi.2012.09.019
2. Wang, Y., Song, S., Xu, C., Hu, N., Molenda, J., Lu, L.: Nano Materials Science. **1**(2), 91–100 (2019). https://doi.org/10.1016/j.nanoms.2019.02.007
3. Bai, P., Han, X., He, Y., Xiong, P., Zhao, Y., Sun, J., Xu, Y.: Energy Storage Materials **25**, 324–333 (2020). https://doi.org/10.1016/j.ensm.2019.10.006
4. Hakim, C., Sabi, N., Saadoune, I.: (2021). Journal of Energy Chemistry. https://doi.org/10.1016/j.jechem.2021.02.027
5. Pan, H., Hu, Y.S., Chen, L.: Energy Environ Sci **6**, 2338–2360 (2013). https://doi.org/10.1039/C3EE40847G
6. Sun, Y., Shi, P., Chen, J., Wu, Q., Liang, X., Rui, X., … & Yu, Y. (2020). EnergyChem, 2(2), 100031. https://doi.org/10.1016/j.enchem.2020.100031
7. Kim, J.K., Lee, E., Kim, H., Johnson, C., Cho, J., Kim, Y.: (2014). ChemElectroChem, 2(3). https://doi.org/10.1002/celc.201402344
8. Noor, S.A.M., Howlett, P.C., MacFarlane, D.R., Forsyth, M.: Electrochim. Acta **114**, 766–771 (2013). https://doi.org/10.1016/j.electacta.2013.09.115
9. Fukunaga, A., Nohira, T., Kozawa, Y., Hagiwara, R., Sakai, S., Nitta, K., et al.: J Power Sources **209**, 52–56 (2012). https://doi.org/10.1016/j.jpowsour.2012.02.058
10. Ponrouch, A., Dedryv_ere, R., Monti, D., E.Demet, A., Ateba, J.M., Croguennec, L., et al.: Energy Environ Sci **6**, 2361–2369 (2013). https://doi.org/10.1039/C3EE41379A
11. Sawicki, M., Shaw, L.: RSC Adv **5**, 53129–53154 (2015). DOI:10.1039/C5RA08321D
12. Es-soufi, H., Bih, L.: J. Non-Cryst. Solids **558**, 120655 (2021). https://doi.org/10.1016/j.jnoncrysol.2021.120655
13. Yabuuchi, N., Kubota, K., Dahbi, M., Komaba, S.: Research Development on Sodium-Ion Batteries. Chem. Rev. **114**, 11636–11682 (2014). https://doi.org/10.1021/cr500192f
14. Liang, Y., Lai, W.H., Miao, Z., Chou, S.L.: Small. **14**(5), 1702514 (2018). https://doi.org/10.1002/smll.201702514
15. Noor, S.A.M., Howlett, P.C., MacFarlane, D.R., Forsyth, M.: Electrochim. Acta **114**, 766–771 (2013). https://doi.org/10.1016/j.electacta.2013.09.115
16. Fukunaga, A., Nohira, T., Kozawa, Y., Hagiwara, R., Sakai, S., Nitta, K., et al.: J Power Sources **209**, 52–56 (2012). https://doi.org/10.1016/j.jpowsour.2012.02.058
17. Fergus, J.W.: Solid State Ionics **227**, 102–112 (2012). https://doi.org/10.1016/j.ssi.2012.09.019

18. Il Kim, J., Choi, Y.G., Ahn, Y., Kim, D., Park, J.H.: J. Mem. Sci. **619**, 118771 (2021). https://doi.org/10.1016/j.memsci.2020.118771
19. Adriana, M.. Nieto-Mu~noz, Jairo, F., Ortiz-Mosquera, Ana, C.M., Rodrigues: Electrochim. Acta **319**, 922–932 (2019). https://doi.org/10.1016/j.electacta.2019.07.032
20. Wu, J. F., Zhang, R., Fu, Q. F., Zhang, J. S., Zhou, X. Y., Gao, P., … & Guo, X. (2021). Advanced Functional Materials, 31(13), 2008165. https://doi.org/10.1002/adfm.202008165
21. Melling, P.J., Allnatt, A.R.: J. Non-Cryst. Solids. **42**(1-3), 553–559 (1980). https://doi.org/10.1016/0022-3093(80)90054-X
22. Fernández, E., Gil, F.J., Ginebra, M.P., Driessens, F.C.M., Planell, J.A., Best, S.M.: J. Mater. Sci. Mater. Med. **10**(3), 169–176 (1999). https://doi.org/10.1023/A:1008937507714
23. Ebendorff-Heidepriem, H., Seeber, W., Ehrt, D.: (1993). Journal of non-crystalline solids, 163(1), 74–80. https://doi.org/10.1016/0022-3093(93)90647-G
24. Reidmeyer, M.R., Day, D.E.: (1995). Journal of non-crystalline solids, 181(3), 201-214. https://doi.org/10.1016/S0022-3093(94)00511-7
25. Pascual, L., Durán, A.: Mater. Res. Bull. **31**(1), 77–95 (1996). https://doi.org/10.1016/0025-5408(95)00152-2
26. Le Sauze, A., Marchand, R., Non-Cryst, J.: Solids 263–264 (2000) 285–292. https://doi.org/10.1016/S0022-3093(99)00673-0
27. Abo-Mosallam, H.A.: J. Non-Cryst. Solids **571**, 121084 (2021). https://doi.org/10.1016/j.jnoncrysol.2021.121084
28. Pershina, S.V., Antonov, B.D., Leonidov, I.I.: J. Non-Cryst. Solids **569**, 120944 (2021). https://doi.org/10.1016/j.jnoncrysol.2021.120944
29. Ibrahim, A., Sadeq, M.S.: (2021). Ceramics International. https://doi.org/10.1016/j.ceramint.2021.07.011
30. Es-soufi, H., Bih, L.: J. Non-Cryst. Solids **558**, 120655 (2021). https://doi.org/10.1016/j.jnoncrysol.2021.120655
31. Es-Soufi, H., Bih, L., Benzineb, M.: New Journal of Glass and Ceramics. **9**(03), 33 (2019). 10.4236/njgc.2019.93004
32. Segawa, H., Akagi, N., Yano, T., Shibata, S.: J. Ceram. Soc. Jpn. **118**, 278–282 (2010). https://doi.org/10.2109/jcersj2.118.278
33. Silva, A.M.B., Correia, R.N., Oliveira, J.M.M., Fernandes, M.H.V.: J. Eur. Ceram. Soc. **30**(6), 1253–1258 (2010). https://doi.org/10.1016/j.jeurceramsoc.2009.11.001
34. Mimouni, I., Bouziani, A., Naciri, Y., Boujnah, M., Belghiti, E., M. A., & Azzouzi, E., M. (2021). Environ. Sci. Pollut. Res., 1–13. https://doi.org/10.1007/s11356-021-16146-w
35. Brauer, D.S.: Angew. Chem. Int. Ed. **54**, 4160–4181 (2015). https://doi.org/10.1002/anie.201405310
36. Kiani, A., Lakhkar, N.J., Salih, V., Smith, J.V.H.M.E., Newport, R.J., Pickup, D.M., Knowles, J.C.: Philos. Trans. R. Soc. A **370**, 1352–1375 (2012). https://doi.org/10.1098/rsta.2011.0276

37. Abou Neel, E.A., Chrzanowski, W., Knowles, J.C.: Acta Biomater **4**, 523–534 (2008). https://doi.org/10.1016/j.actbio.2007.11.007
38. Kasuga, T., Abe, Y., Non-Cryst, J., Solids: 243 (1999) 70–74. https://doi.org/10.1016/S0022-3093(98)00820-5
39. Kaur, M., Singh, A., Thakur, V., Singh, L.: J. Mol. Struct. **1089**, 95–10 (2015). https://doi.org/10.1016/j.molstruc.2015.02.012
40. Ataalla, M., Afify, A.S., Hassan, M., Abdallah, M., Milanova, M., Aboul-Enein, H.Y., Mohamed, A.: J. Non-Cryst. Solids **491**, 43–54 (2018). https://doi.org/10.1016/j.jnoncrysol.2018.03.050
41. Rao, K.: Structural Chemistry of Glasses. Elsevier (2002)
42. Nalin, M., Poirier, G., Ribeiro, S.J.L., Messaddeq, Y., Cescato, L.: Glasses in the $SbPO_4$–WO_3 system. J. Non-Cryst. Solids. **353**, 1592–1597 (2007). https://doi.org/10.1016/j.jnoncrysol.2007.01.031
43. Boudlich, D., Bih, L., Archidi, M.E.H., Haddad, M., Yacoubi, A., Nadiri, A., Elouadi, B.: J. Am. Cer. Society. **85**(3), 623–630 (2002). https://doi.org/10.1111/j.1151-2916.2002.tb00141.x
44. Bih, L., Abbas, L., Azrour, M., El Amraoui, Y., Nadiri, A.: J. ther. Anal. calorimetry. **81**(1), 57–60 (2005). https://doi.org/10.1007/s10973-005-0745-z
45. Rezikyan, A., Moore, G.G.: J. Phys.: Condens. Matter. **32**(48), 485402 (2020)
46. Freschi, C.D., Gouveia, J.T., Marcondes, L., Ferrari, J.L., Cassanjes, F.C., Poirier, G.: Materials Research **20**, 502–508 (2017). https://doi.org/10.1590/1980-5373-MR-2016-0265
47. Pagoti, R., Panda, S., Patchapureddy, V., Padhi, R.K., Subramanian, B., Jena, H., Panigrahi, B.S.: (2021). LUMINESCENCE
48. Nagarjuna, M., Satyanarayana, T., Gandhi, Y., Veeraiah, N.: J. Alloys Compd. **479**(1-2), 549–556 (2009). https://doi.org/10.1016/j.jallcom.2008.12.132
49. Brow, R.K., Tallant, D.R., Myers, S.T., Phifer, C.C.: J. Non-Cryst. Solids **191**, 45–55 (1995). https://doi.org/10.1016/0022-3093(95)00289-8
50. Černošek, Z., Chládková, M., Holubová, J.: J. Non-Cryst. Solids **531**, 119866 (2020). https://doi.org/10.1016/j.jnoncrysol.2019.119866
51. Delahaye-Carrière, F.: (1997). (Doctoral dissertation, Compiègne)
52. C. Solenn. thèse de doctorat, Université Rennes 1, 2016
53. Mascaraque, N., Durán, A., Muñoz, F.: Effect of fluorine and nitrogen on the chemical durability of lithium phosphate glasses. J. Non-Cryst. Solids. **417**, 60–65 (2015). https://doi.org/10.1016/j.jnoncrysol.2015.03.019
54. Es-soufi, H., Bih, L.: J. Non-Cryst. Solids **558**, 120655 (2021). https://doi.org/10.1016/j.jnoncrysol.2021.120655
55. Es-Soufi, H., Bih, L., Benzineb, M.: (2019). Study of Tungsten Phosphate Glasses Containing Fe_2O_3. New Journal of Glass and Ceramics, 9(03), 33.https://doi.org/10.4236/njgc.2019.93004[57] Poluektov, P. P., Schmidt, O. V.
56. Kissinger, H.E.: Journal of research of the National Bureau of Standards **57**, 217 (1956)

57. Augis, J.A., Bennett, J.E.: Journal of thermal analysis. **13**(2), 283–292 (1978). https://doi.org/10.1007/BF01912301
58. Lide, D.R. (ed.): CRC Handbook of Chemistry and Physics. CRC Press, Boca Raton (2001)
59. Avrami, M.: J. Chem. Phys. **7**(12), 1103–1112 (1939). https://doi.org/10.1063/1.1750380
60. Avrami, M.: J. Chem. Phys. **8**(2), 212–224 (1940). https://doi.org/10.1063/1.1750631
61. Avrami, M.: Journal of chemical physics **9**, 177–184 (1941). https://doi.org/10.1063/1.1750872
62. Elkhoshkhany, N., Syala, E.: Ceram. Int. **43**(8), 6156–6162 (2017). https://doi.org/10.1016/j.ceramint.2017.02.011

Figures

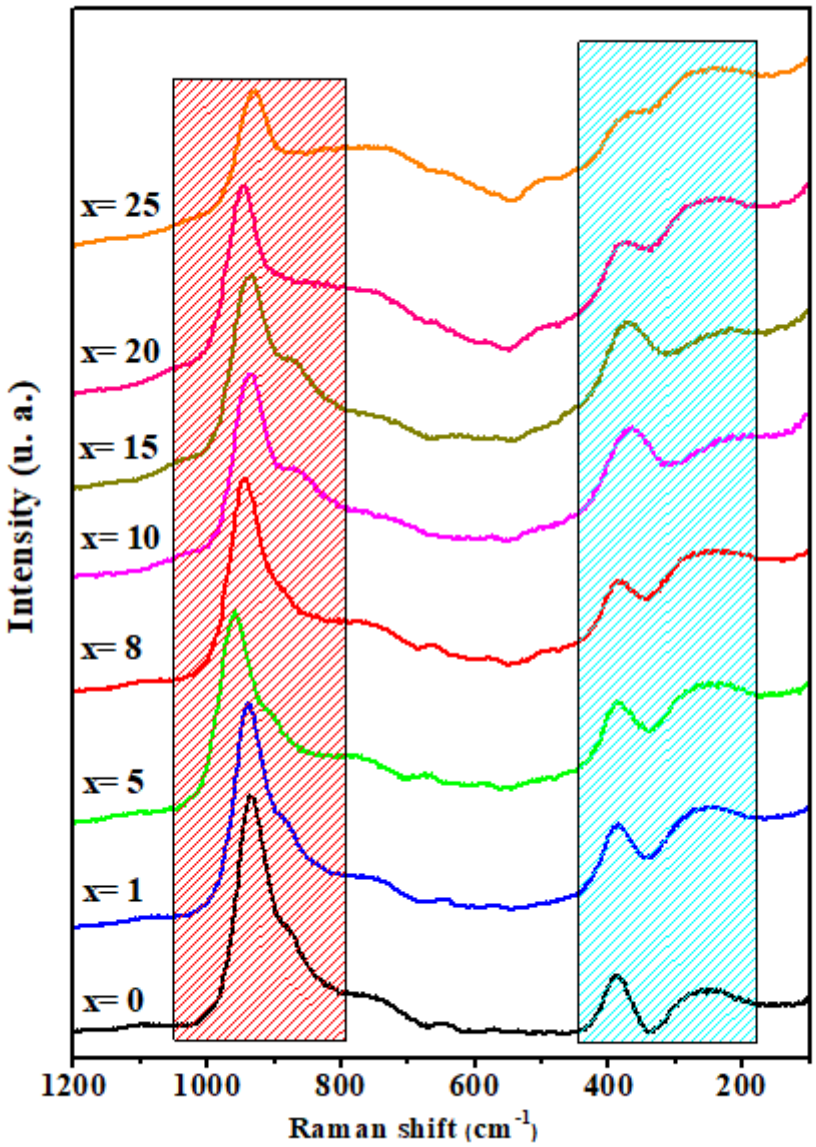

Figure 1

Raman spectra of the studied glasses

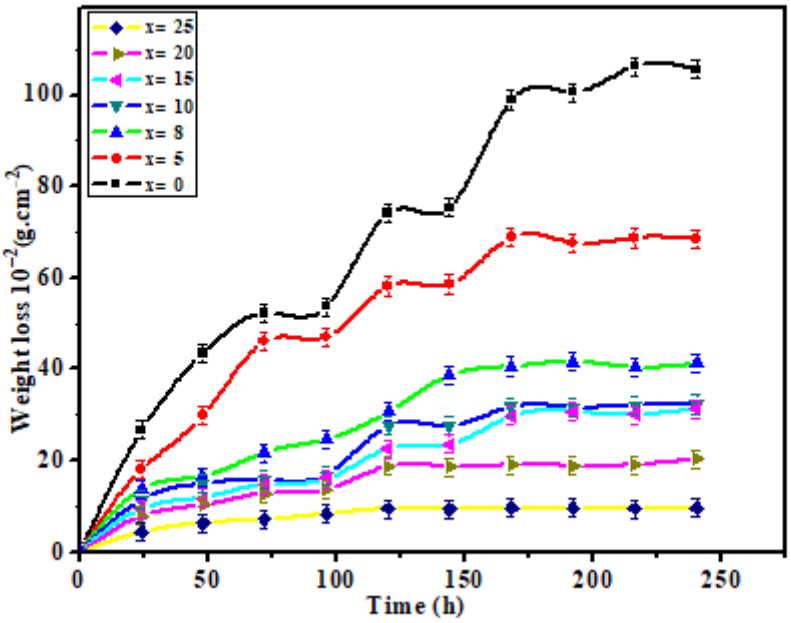

Figure 2

Evolution of the weight loss of the glasses as a function of time (h)

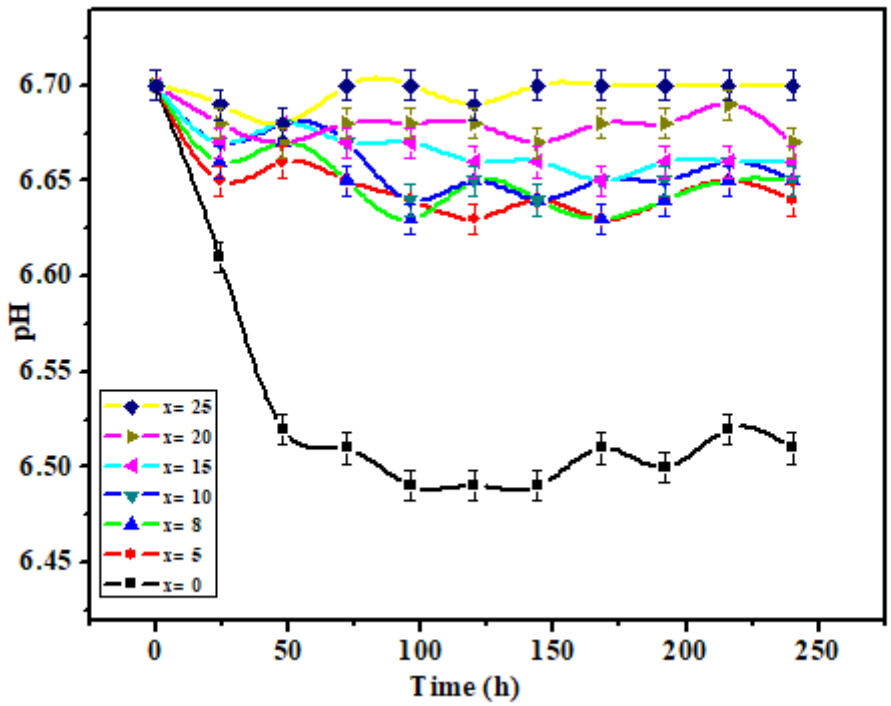

Figure 3

Evolution of the pH of the glasses as a function of time (h)

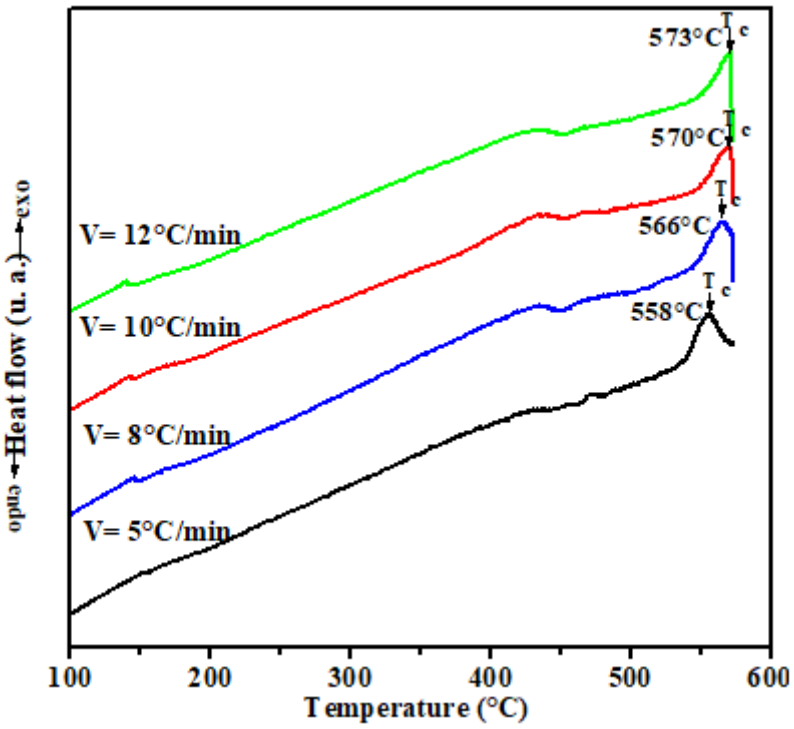

Figure 4

DSC curves for the glass (x = 5) under different heating rates

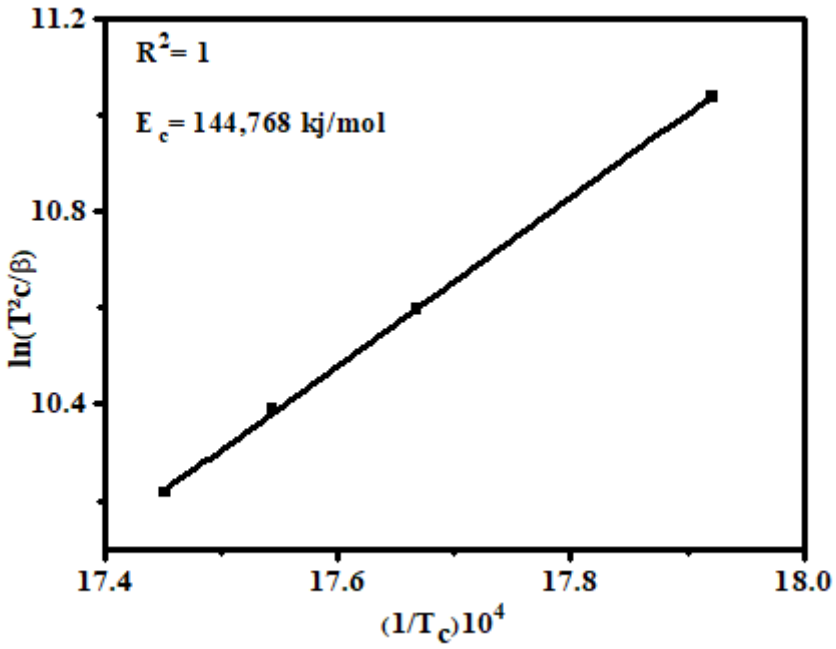

Figure 5

Plot of ln(T2p/b) versus inverse temperature for the glass